The 3-D Thermal Structure of the Helvetic Nappes of the European Alps: Implications for Collisional Processes

Jean Baptiste Girault, Nicolas Bellahsen, Alexandre Boutoux, Claudio Rosenberg, U. Nanni, Anne Verlaguet, O. Beyssac

HAL Id: insu-03691315

https://insu.hal.science/insu-03691315

Submitted on 9 Jun 2022

The 3-D Thermal Structure of the Helvetic Nappes of the European Alps: Implications for Collisional Processes

J. B. Girault[1] , N. Bellahsen[1], A. Boutoux[1], C. L. Rosenberg[1], U. Nanni[2] , A. Verlaguet[1], and O. Beyssac[3]

[1]Sorbonne Université, CNRS-INSU, Institut des Sciences de la Terre Paris, ISTeP UMR 7193, Paris, France, [2]Université Grenoble Alpes, Grenoble, France, [3]Institut de Minéralogie, de Physique des Matériaux et de Cosmochimie (IMPMC), UMR 7590 Sorbonne Université, CNRS and MNHN, Campus Jussieu, Paris, France

Abstract Understanding the rheology of orogenic wedges requires the knowledge of the structural and thermal evolution of collisional units. In this study, we document the maximum temperature reached by the sedimentary cover nappes of the External Crystalline Massif (Western and central Alps) by Raman spectroscopy of carbonaceous material, between the Belledonne (France) and the Aar (Switzerland) Massifs. These cover units form the Helvetic/Dauphinois nappe complex. Maximum temperatures reached by the Upper Helvetic nappes lie in a range spanning from below 220 and 350 °C $\pm$ 50 °C. For the Lower Helvetic nappes, the temperatures spread between 226 and 358 °C $\pm$ 50 °C. These temperatures were projected on two structural cross sections in order to constrain the 3-D thermal structure. From these data, we propose that the Helvetic nappes were deformed and emplaced before and/or during the thermal peak, which supports recent findings that shortening in the External Crystalline Massif was mainly accommodated during a 5- to 10-Myr-long thermal peak before deformation localized along crustal thrusts, which exhumed and cooled down the wedge. During this late exhumation, the isotherms corresponding to the thermal peak were passively folded.

1. Introduction

The tectonic style of orogenic wedges is controlled by several factors, such as the number and the mechanical properties of detachment horizons (e.g., Konstantinovskaia & Malavieille, 2005; Yamato et al., 2011), the efficiency of erosion (e.g., Beaumont et al., 1994; Stockmal et al., 2007), and most importantly the geothermal gradient and temperature distribution inside the wedge (e.g., Jamieson et al., 1996, 1998). The thermal structure of orogenic wedges mainly depends on the radiogenic heat production, on erosion rates, on the thermal diffusivity, and on the rates of convergence (e.g., Jamieson et al., 1996, 1998). Each of these parameters has been tested by simplified models showing how they affect the temperature distribution in space and time, which in turn affects the localization of deformation, hence the style and architecture of an orogenic wedge (e.g., Liao et al., 2018; Piccolo et al., 2017). The 2-D thermal models (Batt & Braun, 1997; Huerta et al., 1996, 1998; Jamieson et al., 1998; Vanderhaeghe et al., 2003) show the deflection of isotherms during initial thrusting and their upward doming during ongoing thickening on the scale of an orogen. On the scale of individual nappes, thermomechanical models show that the fundamental parameters controlling the tectonic style are the initial geometry of the basins, that is, the geometry of the basement-cover interface and lateral variations in the cover, and the viscosity ratio between cover and basement (e.g., Bauville & Schmalholz, 2015; Lafosse et al., 2016), which is partly controlled by the initial temperature distribution and its evolution during convergence.

Evaluating the effect of temperature, hence rheology, on the present-day geometry of a nappe stack, also requires constraints on the metamorphic *P-T-t* path and the relative chronology of the metamorphic peak and deformation event. Therefore, the absolute age and duration of the thermal peak and its timing relative to the structures accommodating shortening, indicating whether the main deformation event occurs before, during, and/or after the metamorphic peak, need to be constrained.

These results can be used to relate deformation localization to the wedge rheology. For example, in the Oisans External Crystalline Massif (ECM) in the Western Alps (Figure 1), the thermal peak postdated or was coeval with the observed shortening, because a rather flat "isotherm" cutting across nappe-internal
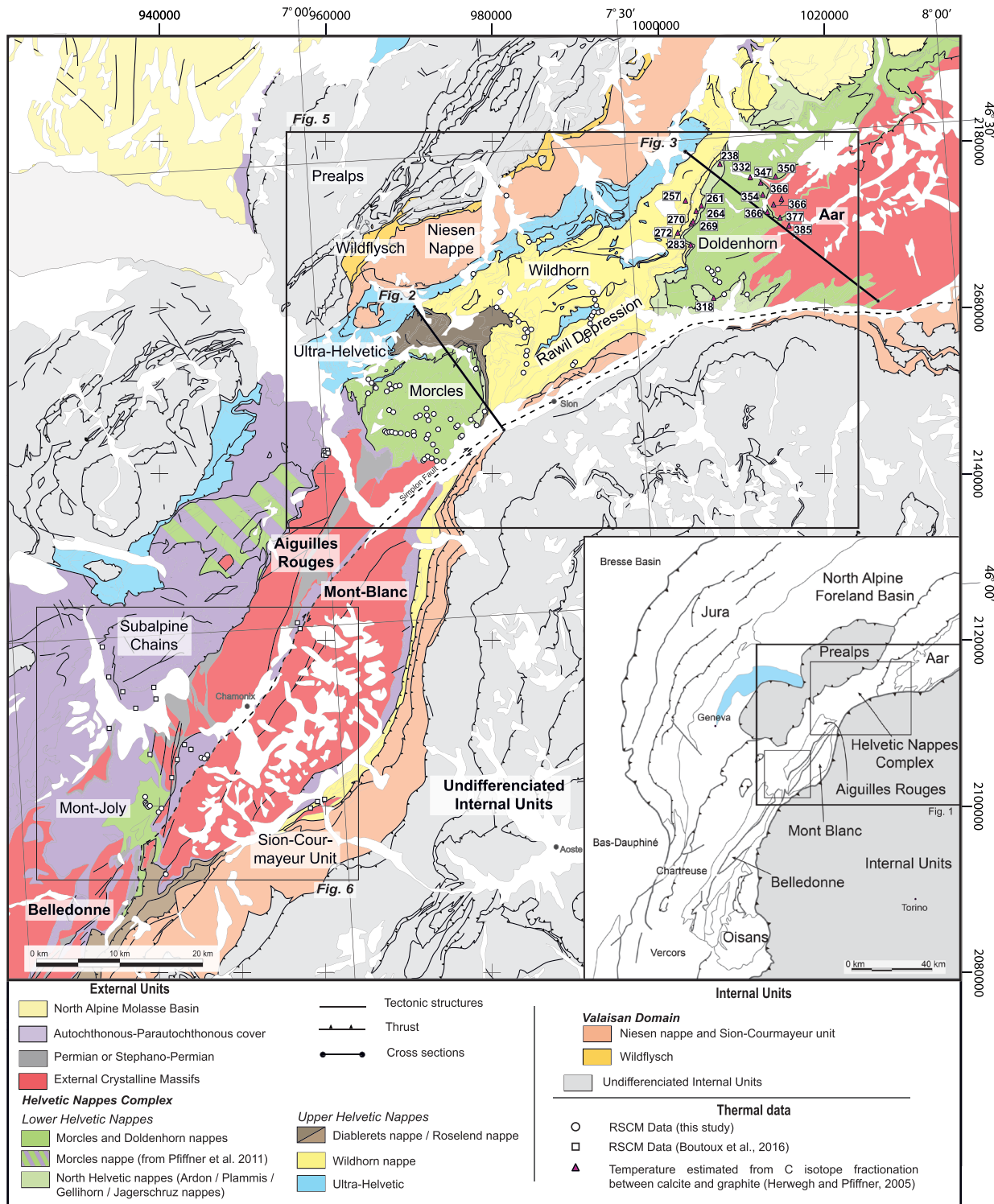
Figure 1. Geological map of the Alpine western arc external units (modified after Debelmas et al., 1980; Broquet et al., 1987; University of Bern and University of Bern and FWOG: Geological map of Switzerland 1:500000, 2005; University of Bern and FWOG: Tectonic Map of Switzerland 1:500 000, 2005; Pfiffner, 2011). External Crystalline Massifs (ECMs), that is, basement of the European proximal margin, are in red. Green, yellow, and brown units are the tectonic cover of the ECM, and the purple units are the sedimentary cover of the ECM. Dots are temperature data from different methods (e.g., C isotope fractionation between calcite and graphite, Herwegh & Pfiffner, 2005; Boutoux et al., 2016), and Raman spectroscopy of carbonaceous material (RSCM) data from this study. Black lines are the location of cross sections presented in Figures 2 and 3. Inset map on the bottom right shows the location at larger scale, gray: internal units, and white: external units.

structure could be documented to have existed during significant shortening and folding of the crust (Bellanger et al., 2015). This suggests that distributed shortening occurred at the temperature peak as also suggested for the Mont Blanc ECM (Boutoux et al., 2016). Similar studies relating the tectonic and the thermal structure in the Helvetic nappes were also performed by Groshong et al. (1984), Herwegh and Pfiffner (2005), and Nibourel et al. (2018).

However, beyond those examples, little is known about the 3-D distribution of temperature in natural orogenic wedges, especially on the scale of sedimentary nappe stacks. Based on compilations of metamorphic temperature conditions, isomaximal temperature (iso-T_{MAX}) lines are often constructed in map view (Bousquet et al., 2008; Engi et al., 2001; Todd & Engi, 1997) and rarely in cross sections (Bousquet et al., 2008; Nibourel et al., 2018). Yet these valuable attempts need to be taken with caution, because the inferred temperature may not have been attained synchronously and because the geometry of the temperature boundaries in map view is usually insufficiently constrained to be soundly interpreted in terms of orientation of a surface at depth. A noticeable exception is the detailed study of Wiederkehr et al. (2011) at the eastern end of the Lepontine dome in the central Alps, where the well-constrained iso-T_{MAX} lines in map view could be used to illustrate the geometry of iso-T_{MAX} lines in cross sections over a vertical interval of approximately 4 km. These results illustrate how a nappe stack and its associated isotherms were formed during Eocene subduction and later folded during collision (Wiederkehr et al., 2011).

In the present study, we investigate the thermal structure of a stack of unmetamorphosed to low grade metamorphic cover nappes that formed in the Helvetic realm of western Switzerland, during collision of the Alpine Chain (Figure 1). We map the surface distribution of iso-T_{MAX} lines across several nappes, based on RSCM analyses on a very dense distribution of samples, and we make use of these lines to construct their geometry at depth. The high topographic relief and the late tilting of the nappes in the study area allow for a reconstruction of the structures at depth (Escher et al., 1993; Huggenberger, 1985; Ramsay & Huber, 1987). These factors allow us to project the inferred T_{MAX} data from the map view into a vertical section over a depth range of approximately 10 km. Therefore, this study provides a 3-D reconstruction of the thermal structure of a syncollisional nappe stack, allowing to visualize and discuss the temporal relationships between nappe formation and metamorphic peak in a natural orogenic wedge.

2. Geological Setting

The Western Alps formed as the result of subduction of the Ligurian Ocean, since the Late Cretaceous and subsequent continental subduction and collision of the European margin during Eocene and Oligo-Miocene times, respectively (e.g., Bucher et al., 2004; Ceriani & Schmid, 2004; Chopin, 1987; Dumont et al., 2012; Fugenschuh & Schmid, 2003; Stampfli et al., 2002). Continental collision between the European proximal margin and the protoorogenic wedge (made of a nappe stack of Briançonnais/Ligurian/Austroalpine units) led to thickening of the European crust, mainly accommodated by two orogen-scale anticlinal dome structures, one forming the internal massifs, the other forming the ECM in the External Zone (e.g., Bellahsen et al., 2014; Burkhard & Sommaruga, 1998; Dumont et al., 2008; Leloup et al., 2005). These domes differ from one another both in terms of structure and metamorphic conditions, but the age of Barrovian metamorphism in both structures is similar. The Lepontine dome consists of a stack of thin basement nappes (Steck et al., 2013), separated by their thin Mesozoic covers series. Some of the nappes record Alpine High-Pressure Low-Temperature metamorphism, in addition to a High Temperature, Barrovian overprint, whose isograds are discordant to all nappe contacts and trace a domal shape. The stacking itself is inferred to be completed in the Late Eocene/Early Oligocene (Schmid et al., 1996) and the peak of HT metamorphism persists until approximately 22 Ma (Rosenberg & Berger, 2009). In contrast, the ECM are formed by series of hinterland dipping basement thrusts, on top of which lies an antiformal stack, solely consisting of cover nappes. The initiation of these basement thrusts is inferred to be Early Oligocene (Bellahsen et al., 2014), and their metamorphic peak is bracketed between 29 and 16 Ma (Boutoux et al., 2016), hence partly coeval with HT metamorphism in the Lepontine, but more persistent through time.

The Triassic to late Eocene/early Oligocene (Pfiffner, 2014) sedimentary cover of the ECM, in which several asymmetric synrift basins of Early to Middle Jurassic age are preserved (e.g., Lemoine et al., 1986), was also shortened during collision (Bellahsen et al., 2012; Boutoux et al., 2016; Burkhard & Sommaruga, 1998; Lemoine et al., 1986).
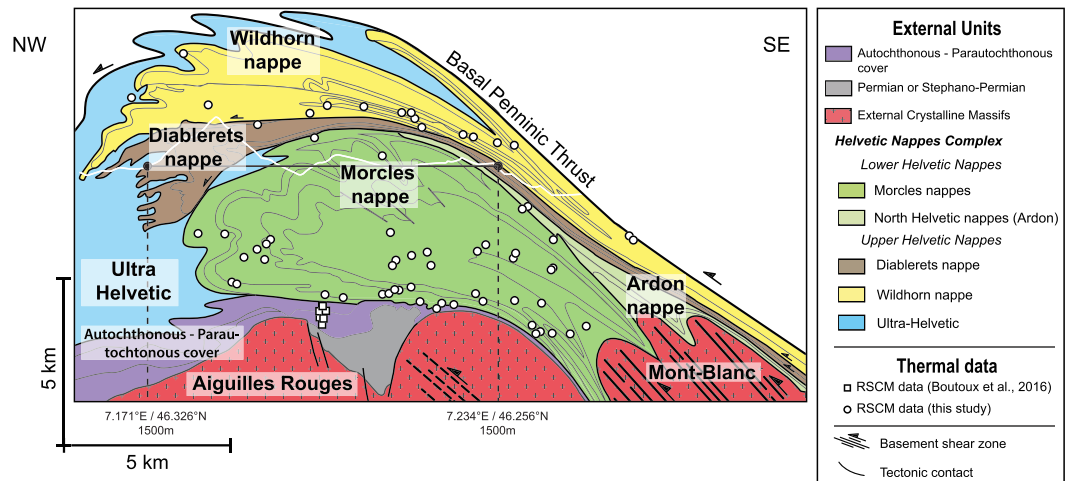
Figure 2. Western cross section of the Helvetic nappe complex (see Figure 1 for location) modified after Escher et al. (1993). Dots indicate the location of samples from Morcles, Diablerets, and Wildhorn nappes after projection parallel to the fold axes.

In the Mont Blanc area, the main structure is a stack of cover nappes, forming the Helvetic nappes in Switzerland and their probable equivalent in France, the Mont Joly (Figure 1). These nappes consist of Mesozoic and Tertiary sedimentary rocks (Upper Triassic to Lower Oligocene; see Pfiffner et al., 2010, for review). Mesozoic (meta) sediments mostly form alternations of prerift, synrift, and postrift marls and limestones, whereas Cenozoic sediments constitute flysch-type basins (Sinclair, 1997) and Paleogene Wildflysch in the Ultra-Helvetic Realm, that is, in the most distal part of the European margin.

The geometry of these nappes is very well constrained in western Switzerland (Figures 1–3; Escher et al., 1993; Huggenberger, 1985). Late uplift (see below) of the underlying Aar and Mont Blanc ECM resulted
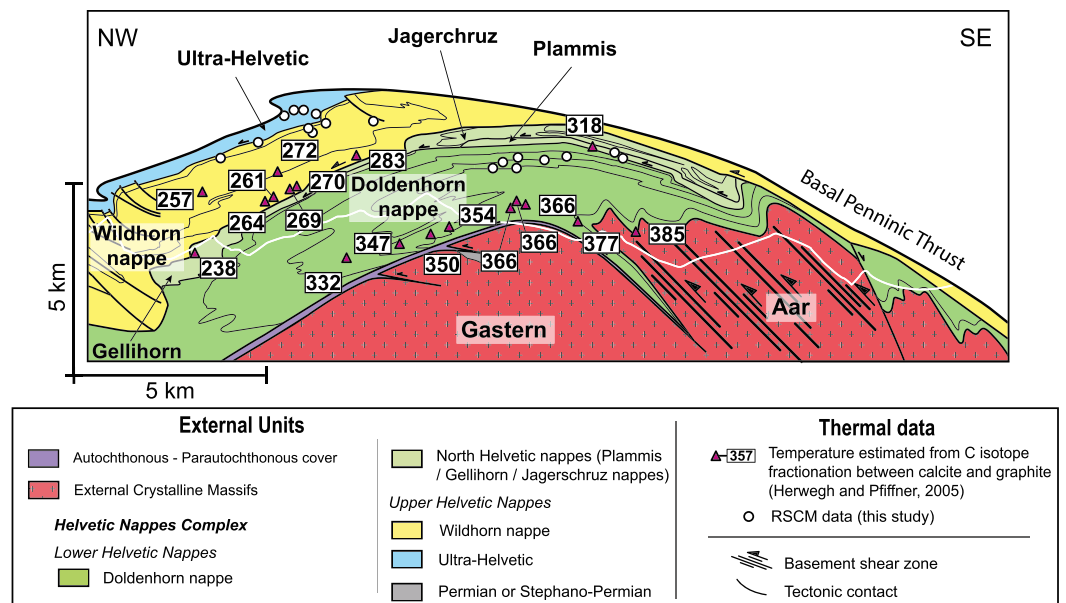
Figure 3. Eastern cross section of the Helvetic nappe complex (see Figure 1 for location) after Burkhard (1988) and Pfiffner (2011). Dots indicate the location of samples used in this study following the projection parallel to the fold axes, as well as sample location from Herwegh and Pfiffner (2005).
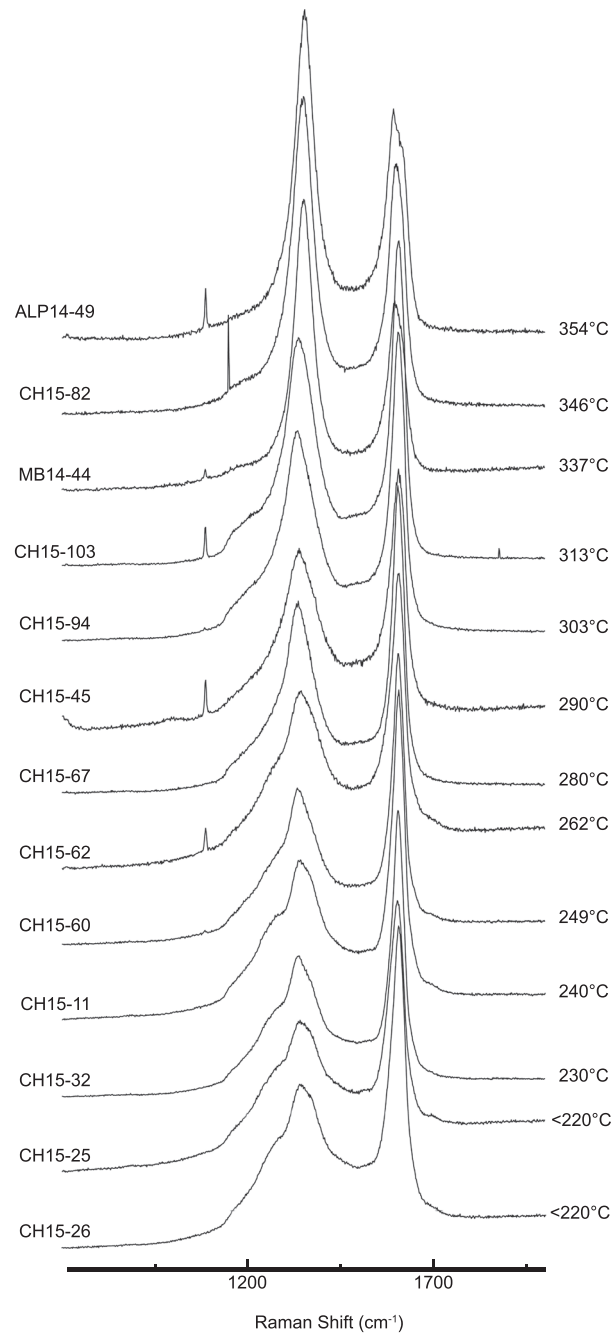
Figure 4. Selection of representative Raman spectra of carbonaceous material (CM) obtained in various units of the Helvetic nappe complex indexed by increasing metamorphic grade. See Beyssac, Goffé, et al. (2002) and Lahfid et al. (2010) for details regarding RSCM thermometry. For very disordered graphitic carbon that is found in least metamorphosed rocks, we assign $T < 220$ °C.

in tilting of their covers, hence allowing for axis-parallel projection of structures in cross sections. This enables the reconstruction of the nappe stack over a vertical distance of >10 km (Figure 2; e.g., Escher et al., 1993), showing that three major cover nappes are piled over the Mont Blanc-Aiguilles Rouges Massif (Figure 2) and over the Aar Massif (Figure 3). Above the Mont Blanc-Aiguilles Rouges Massif, these nappes are from top to bottom, the Wildhorn, the Diablerets, and the Morcles/Ardon nappes. The Wildhorn and the Diablerets nappes are completely detached from their basement (Figure 2) that is inferred to be located

further SE at depth (Kempf & Pfiffner, 2004; Pfiffner, 2014). In contrast, the Morcles nappe, in spite of a long and stretched inverse limb that overlies the Aiguilles Rouges basement (Figure 2), shows that its folded core is still attached to its folded basement, represented by the Mont Blanc Massif (Figure 2). The upper nappes are characterized by recumbent folds at their fronts, but the lower limbs are either poorly developed or lacking altogether above discrete thrust contacts with underlying nappes (Figure 2).

In contrast, the Morcles nappe, forms a large, recumbent isoclinal fold, in which the inverted and the normal limbs have the same length, attaining over 10 km (Figure 2). A similar structural trend is observed further east, above the Aar-Gastern Massif (Figure 3), where the lower nappe (Doldenhorn nappe), although far transported to the north, still shows a coherent, folded depositional contact with underlying basement (Figure 3), and consists of a recumbent, isoclinal fold, with a long, well-developed inverted limb. SW of the Mont Blanc Massif, the Mont Joly nappe (Figure 1) is interpreted as structurally equivalent to the Morcles nappe. The uppermost nappes (Wildhorn, as well as the intermediate ones: Gellihorn/Jagerchruz/Plammis) are entirely detached from their basement and do not show any inverted lower limb (Figure 3).

The entire pile of Helvetic and Ultrahelvetic cover nappes lies below the basal Penninic thrust, which forms the base of the Penninic units. The latter units crop out to the NW (Préalpes) and SE of the Helvetic nappes (internal zone) and were completely eroded above the large scale antiformal stack of the Helvetic nappes. The structure of the internal units consists of a nappe sequence, derived from bottom to top from the Valaisan Domain, the Briançonnais continental sliver, and the Liguro-Piemont oceanic domain. Thrusting of these internal units over the Helvetic nappes occurred from late Eocene to early Oligocene time (Pfiffner, 1993; Schmid et al., 1996; von Tscharner et al., 2016), hence to have induced metamorphism of the European nappes in their footwall. The metamorphic peak of the ECM and the amount of shortening of the alpine External zone increase from south to north (e.g., Bellahsen et al., 2014). In the south of the arc, in the Oisans Massif (Figure 1, inset), the collisional P-T peak conditions attained 350 °C $\pm$ 50 °C and 3.5 kbar $\pm$ 1 kbar (Bellanger et al., 2015) with a total shortening for the external zone of 28 km (internal deformation of the ECM, i.e., distributed shear zones, and thrusting along frontal ramp; Bellahsen et al., 2014). In the Oisans ECM, the thermal peak and the shortening lasted between 30 and 25 Ma (Bellanger et al., 2015). For the Mont Blanc Massif (Figures 1 and 2), thermobarometric data from shear zone samples indicate a metamorphic peak at 400 °C $\pm$ 25 °C and 5 kbar $\pm$ 0.5 kbar (Rolland et al., 2008); shortening of the external zone there attained some 66 km (internal deformation including the Mont Blanc shear zone and frontal ramps; Bellahsen et al., 2014). In the Mont Blanc ECM, the thermal peak and the main phase of shortening lasted between 30 and 18 Ma (Boutoux et al., 2016). Further north, in the Aar Massif shear zones (Figures 1 and 3), the metamorphic peak is estimated at 450 °C $\pm$ 50 °C and 6 kbar $\pm$ 1 kbar (Challandes et al., 2008; Goncalves et al., 2012; Rolland et al., 2009) with a total shortening of 69 km (Burkhard, 1988).

The distribution of metamorphic temperatures in the cover (e.g., Morcles nappe, Burkhard & Goy-Eggenberger, 2001 and Oisans Massif, Crouzet et al., 1999, Bellanger et al., 2015) shows a crosscutting pattern between stratigraphic layers and iso-T_{MAX} lines. The Morcles nappe reached a temperature peak corresponding to the diagenetic zone ($T_{MAX} < 200$ °C) in its frontal parts and the epizone in the rear of the nappe, both in the normal and inverted limbs ($T_{MAX} > 300$ °C, Kirschner et al., 1995, Burkhard & Goy-Eggenberger, 2001). According to Herwegh and Pfiffner (2005) similar P-T conditions were assessed in the eastern, lower Helvetic nappes (Doldenhorn nappe). Maximum temperatures there range from 180 °C in the frontal part, to 380 °C, in the SW, close to its basement.

The timing and sequence of shortening of the External Zone are well documented. Distributed shortening in the ECM is coeval with the thermal peak, as detailed above. In the Mont Blanc area, most of the distributed shortening took place between 30 and 17 Ma, although some deformation occurred later (see Boutoux et al., 2016, and references therein). At 17 Ma, crustal thrust ramps initiated below the Aiguilles Rouges Massifs, exhuming the ECM as attested by the cooling recorded by thermochronometers (e.g., Boutoux et al., 2016; Egli & Mancktelow, 2013; Fugenschuh & Schmid, 2003; Glotzbach et al., 2008, 2010, 2011; Leloup et al., 2005; Michalski & Soom, 1990; Rahn, 2001; Seward & Mancktelow, 1994) and the activation of cover thrusts in the basin (Burkhard & Sommaruga, 1998). At the end of the Miocene, another crustal ramp initiated and activated the décollement below the Jura (e.g., Burkhard & Sommaruga, 1998).

3. Methodology

Sampling for RSCM thermometry analyses was performed in the Helvetic and Ultra-Helvetic nappes, within metasediments of Jurassic to Eocene age. These marly to calcareous metasediments contain some carbonaceous material (CM), which permits the assessment, by RSCM thermometry, of the maximum temperature attained by these rocks. Indeed, with burial and temperature increase, organic matter originally deposited in sediments is progressively transformed into graphite. This process is irreversible and thus records the maximum temperature (T_{MAX}) experienced by the rock during *P-T* loops (Beyssac et al., 2002; Beyssac et al., 2002).

The CM is localized preferentially near crystals of pyrite and sometimes trapped in them. The formation of veins by pressure-dissolution process also leads to measurable concentrations of CM near vein boundaries.

The RSCM is based on the quantitative determination of the degree of graphitization of CM, measured from Raman spectra. In a spectral window from 700 to 2,000 cm^{-1}, the Raman spectra can be divided into a graphite band (G) and several defect bands (D1, D2, D3, and D4) attributed to physicochemical defects. The relative area of these bands reflects the degree of graphitization (see Beyssac et al., 2003, and references therein). It can be quantified using the R2 parameter, defined as the relative area of the main defect bands (R2 = D1/(G + D1 + D2)) (Beyssac, Goffé, et al., 2002). These authors proposed an empirical thermometer, which links R2 to T_{MAX} for a temperature range of 330 to 640 °C with an intrinsic calibration error of $\pm$50 °C due to uncertainties on petrologic data used for the calibration. The relative uncertainties on temperature are much smaller, in the range 10–15 °C (Beyssac et al., 2004), allowing for a precise estimate of thermal metamorphic gradients. At lower temperatures, Lahfid et al. (2010) have showed that the evolution of the Raman spectra of CM under low-grade metamorphism in the Glarus Alps (Switzerland) is highly correlated with the peak metamorphic temperature in the range of 220–330 °C. They established a correlation between parameters extracted from the Raman spectra and peak temperatures estimated from independent methods. It is important to note that the fitting method is different at low temperature compared with the original approach by Beyssac, Goffé, et al. (2002), because the spectra are more complex with two more defect bands, D3 and D4 (Lahfid et al., 2010). Here T_{MAX} is estimated using the RA1 parameter (RA1 = (D1 + D4)/(G + D1 + D2 + D3 + D4)), with an intrinsic calibration error of $\pm$25 °C (Lahfid et al., 2010) in the range 220–330 °C. Below 220 °C, the temperature is poorly constrained in Lahfid et al. (2010) as it relies on only one single sample so we adopt a conservative approach and we attribute a value <220 °C.

Raman spectra were obtained using a Renishaw InVIA Reflex microspectrometer (IMPMC Paris). We used a 514.5-nm DPSS Cobolt laser in circular polarization. The laser was focused on the sample by a DMLM Leica microscope with a 100X objective (NA = 0.85) yielding a spot size of ~1 μm. The laser power at the sample surface was set below 1 mW. The Rayleigh diffusion was eliminated by edge filters, and the signal was finally dispersed using an 1,800 grooves per millimeter grating and analyzed by a Peltier cooled RENCAM CCD detector. Before each session, the spectrometer was calibrated with silicon standard. Because Raman spectroscopy of CM can be affected by several analytical mismatches, we followed closely the analytical and fitting procedures described by Beyssac, Goffé, et al., 2002, Beyssac et al., 2003). Measurements were made on polished thin sections, and CM was systematically analyzed below a transparent adjacent mineral, generally quartz. For each sample 10–20 spectra were generally recorded in the extended scanning mode (700–2,000 cm^{-1}). Spectra were then processed using the software Peakfit following the fitting procedures of both Beyssac, Goffé, et al., 2002, Beyssac et al., 2003) and Lahfid et al. (2010). As our samples experienced their temperature peak in the overlap range of the two calibrations described above, T_{MAX} was determined for each sample from the mean peak ratio (R2 or RA1) with the procedure giving the best fit and following the advices given by Lahfid et al. (2010).

4. Results

Temperatures resulting from this RSCM study are displayed in Table S1 (see supporting information), and Figures 4–8 and provide estimates of the T_{MAX} from <220 to 387 °C for the Helvetic complex. The sample locations have been projected parallel to the trend and dip values of fold axes from the 1/50,000 Swiss maps of the Helvetic nappes, from the map on two cross sections (Figures 7 and 8). All samples located west of the
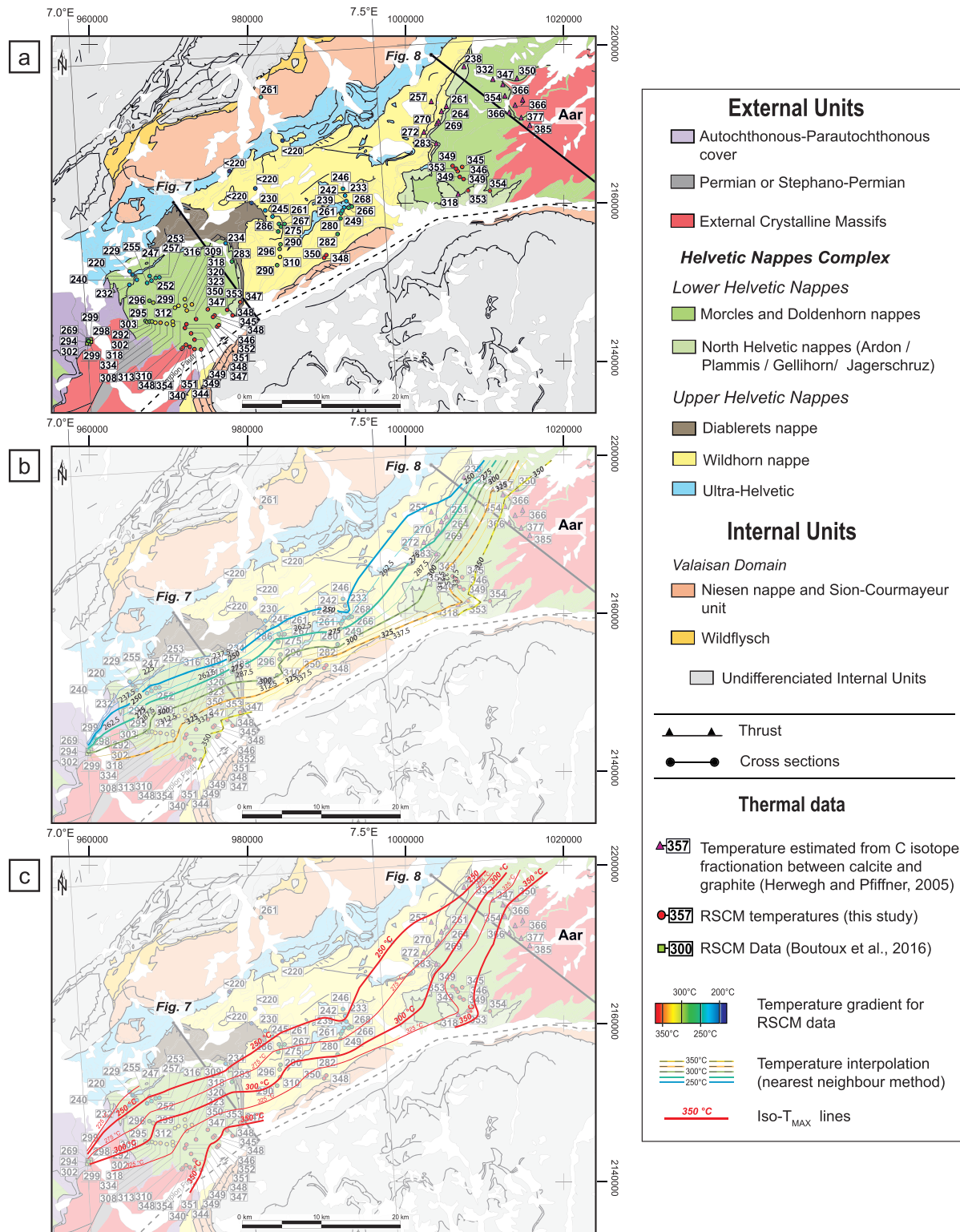
Figure 5. Geological map (modified after University of Bern and University of Bern and FWOG: Geological map of Switzerland 1:500000, 2005, University of Bern and FWOG: Tectonic Map of Switzerland 1:500 000, 2005; Broquet et al., 1987; Debelmas et al., 1980) of the Helvetic nappe complex showing (a) peak metamorphic temperatures estimated by RSCM thermometry from this study and temperature data from different methods (see supporting information Table S1). Cross sections are presented in Figures 7 and 8. (b) Temperature interpolation from MatLab software (nearest neighbor method). (c) Iso-T_{MAX} lines are displayed according to RSCM temperatures from this study and completed with thermochronological data in Soom (1990), Rahn (1994), Seward and Mancktelow (1994), Fugenschuh and Schmid (2003), Leloup et al. (2005), Glotzbach et al. (2008, 2011), Valla et al. (2012), and Boutoux et al. (2016).

AGU
100
ADVANCING EARTH
AND SPACE SCIENCE

Tectonics

10.1029/2018TC005334
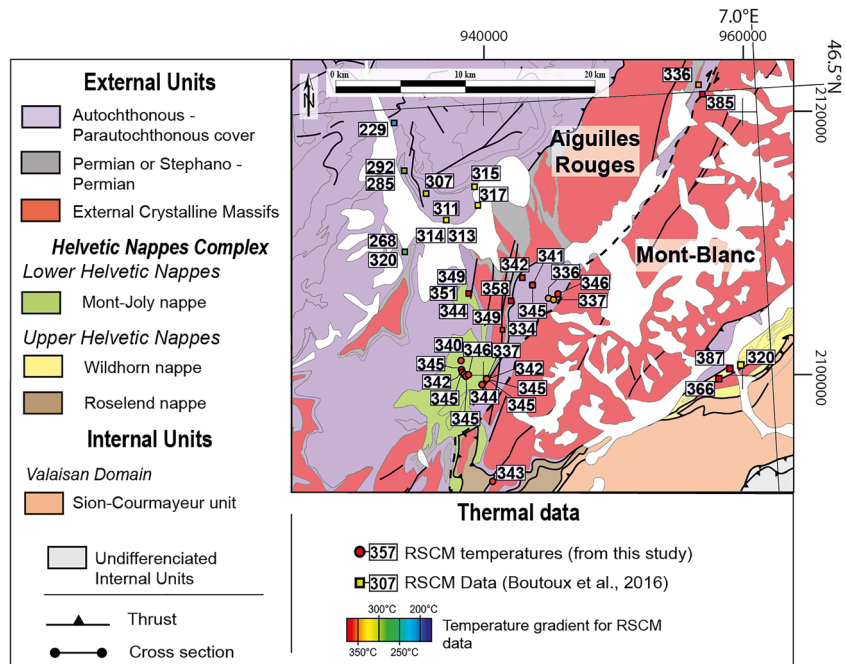
Figure 6. Geological map (modified after University of Bern and University of Bern and FWOG: Geological map of Switzerland 1:500000, 2005, University of Bern and FWOG: Tectonic Map of Switzerland 1:500 000, 2005; Broquet et al., 1987) of the Mont-Blanc and Aiguilles Rouges Massifs and the Lower Dauphinois nappe showing peak metamorphic temperatures estimated by RSCM thermometry from this study (see supporting information Table S1) and from Boutoux et al. (2016).

Rawil depression were projected on the cross section of Figure 7, and all the ones located east of the Rawil depression were projected on the section of Figure 8. In the Morcles nappes (Figures 5a and 7a), T_{MAX} is in the range between <220 and 354 °C. The normal limb of the Morcles nappe exhibits temperatures between 234 and 352 °C. The inverse limb shows temperatures between 232 and 354 °C, with temperature decreasing toward the hinge region, that is, from SE to NW in map view (Figure 6a). Within the inner part of the Morcles nappe, temperatures are higher and spread from 340 to 354 °C. In the northwestern frontal part, temperatures are lower and in the range from <220 to 268 °C. In the overlying Diablerets nappe (Figures 5a and 7a) only one T_{MAX} was obtained, corresponding to 206 °C. In the Wildhorn nappe (Figures 5a and 7a) T_{MAX} range between 233 and 350 °C.

In the Doldenhorn nappe (Figures 5a and 8a), our T_{MAX} data are located in the internal part of the normal limb, and they vary between 344 and 358 °C. These values are similar to those from the inner part of the Morcles nappe (i.e., 340–354 °C). In the Wildhorn nappe, the T_{MAX} range between 344 and 358 °C. A temperature decrease from SE to NW is observed as for the Lower Helvetic nappes.

Southwestward, in the Mont Joly nappe (considered as a Lower Dauphinois nappe), temperatures reached between 226 and 356 °C (Figure 6). As in the Helvetic nappes, the temperature decreases from SE to NW.

In the Ultra-Helvetic nappes (Figures 5a, 7a, and 8a), temperatures in the range between <220 and 261 °C.

In the Penninic units, east to the Mont-Blanc Massif, three samples from the Valaisan domain (Sion-Courmayer Unit) provide temperatures between 320 and 387 °C (Figure 6) and one sample from the Niesen nappe, also derived from the Valaisan Domain (NE), yields 261 °C (Figure 5a).

The above determined temperature data were interpolated in map view and cross section (Figures 5b, 7b, and 8b), thus defining pattern of iso-T_{MAX} lines (Figures 5c, 7c, and 8c). The interpolation was performed using a Matlab routine (nearest neighbor algorithm). In map view, results show that iso-T_{MAX} lines strike ENE and cross cut the nappe boundaries (Figure 5a). Only at the western end of the Aar Massif a marked deflection from the ENE strike is observed and iso-T_{MAX} lines rotate locally into a NW orientation. In the
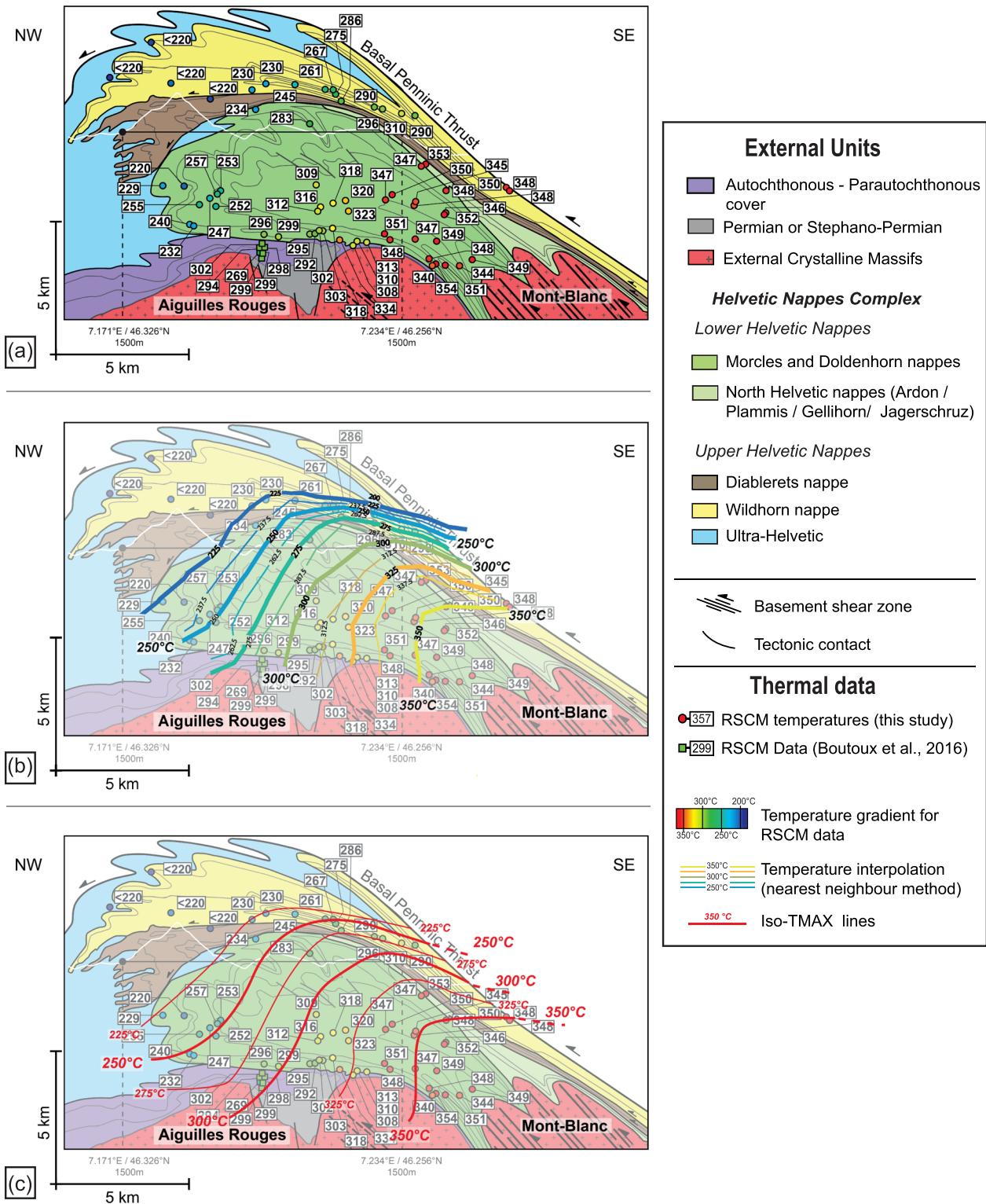
Figure 7. Western cross section of the Helvetic nappes complex (see Figure 1 for location) modified after Escher et al. (1993). (a) With RSCM data (see supporting information Table S1) projected parallel to the fold axes. (b) With temperature contour lines interpolated with MatLab software (nearest neighbor method). (c) With iso-T *MAX* lines according to RSCM temperatures from this study.
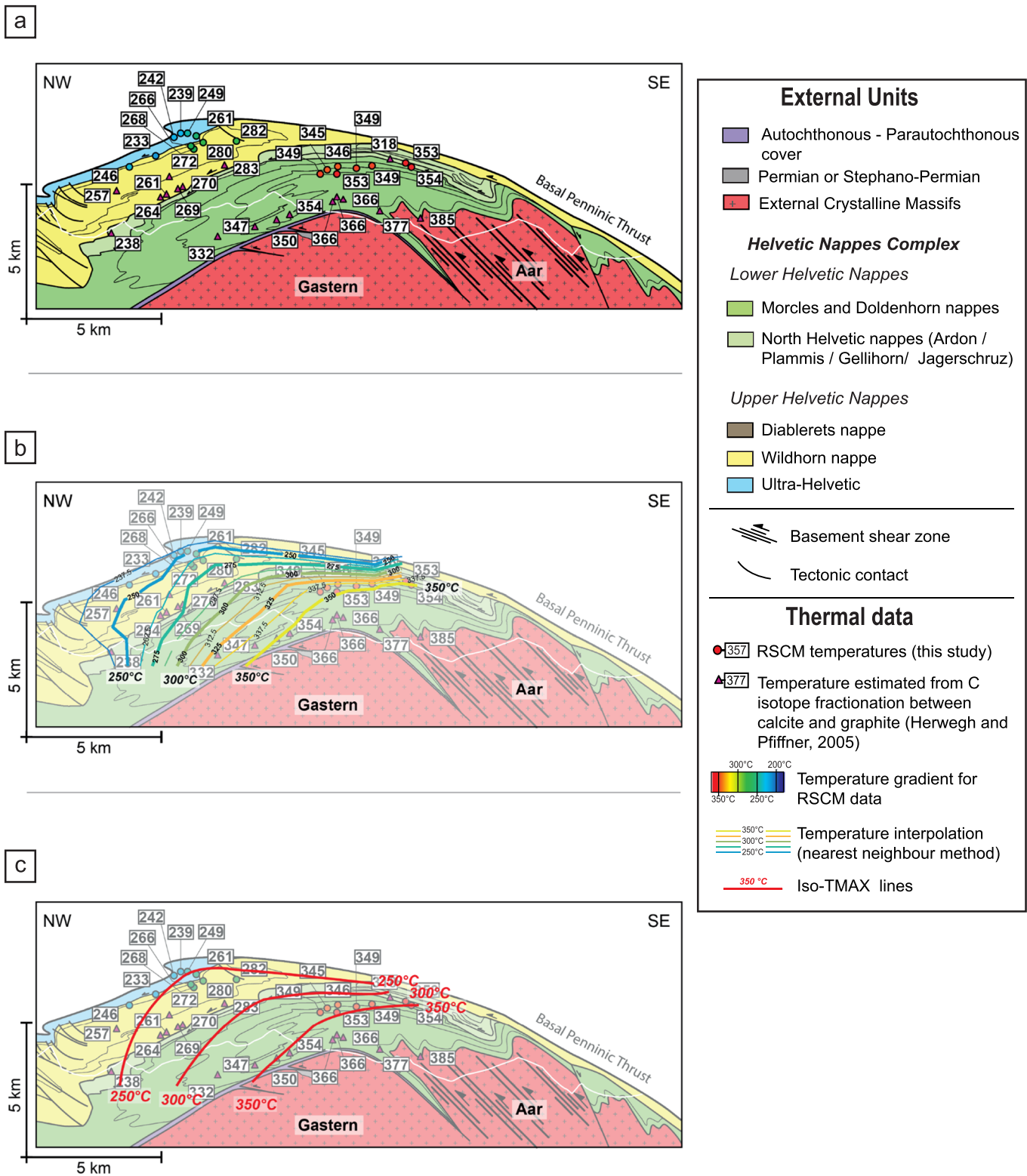
Figure 8. Eastern cross section of the Helvetic nappes complex (see Figure 5 for location) after Burkhard (1988) and Pfiffner (2011). (a) Dots indicate the location of RSCM data used in this study (see supporting information Table S1) and projected parallel to the fold axes, as well as temperature data from Herwegh and Pfiffner (2005). (b) Temperature interpolation performed with MatLab software (nearest neighbor method). (c) Iso-T_{MAX} lines are displayed according to RSCM temperatures from this study.
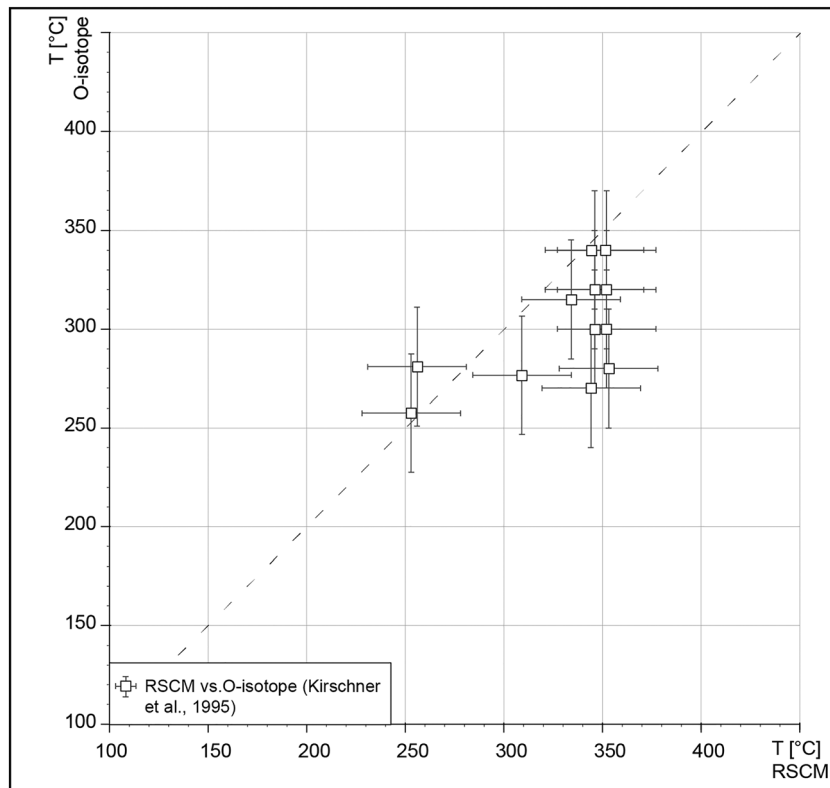
Figure 9. Correlation between RSCM temperature and O-isotope thermometry (Kirschner et al., 1995) on samples located at a maximum of 500 m from each other. See text for details and Table S2 of the supporting information.

western Helvetic nappes, our sampling is denser; hence, the location of the three iso-T_{MAX} lines corresponding to 350, 300, and 250 °C (Figures 5c, 7c, and 8c) can be considered as robust in this area, both within the Lower and the Upper Helvetic nappes. On the contrary, for the eastern Lower Helvetic nappes, only one iso-T_{MAX} line can be drawn based on our own RSCM data, namely, the 350 °C line (Figures 5c and 8c). The other iso T_{MAX} lines are drawn based on temperature data from Herwegh and Pfiffner (2005). The iso-T_{MAX} lines are almost continuous across the contact between Lower and Upper Helvetic nappes.

On both sections, one can see the same results: The iso-T_{MAX} lines crosscut the main nappe contacts. Moreover, the iso-T_{MAX} lines appear folded.

5. Discussion

5.1. Alpine Thermal Peak in the Helvetic Nappes

The range of RSCM T_{MAX} data obtained from the Morcles nappe is consistent with RSCM temperatures from Boutoux et al. (2016).

They are also in good agreement with temperatures derived from quartz-calcite oxygen isotope thermometry performed within synkinematic veins, inferred to have formed at the temperature peak (Figure 9; Kirschner et al., 1995), illite crystallinity data (Burkhard & Goy-Eggenberger, 2001). These techniques revealed temperatures from 240 °C ± 30 °C in the frontal part to 350 °C ± 30 °C in the internal part of the nappe (Kirschner et al., 1995. In general, the temperature differences between the methods are within the uncertainty inherent of each method. However, temperatures from O-isotope (Kirschner et al., 1995) are lower than RSCM temperatures. However, the geometry of the iso-T_{MAX} lines depicted in Figure 7 shows some significant differences compared to the geometry reconstructed by Burkhard and Goy-Eggenberger (2001) on the basis of their illite crystallinity data. Since the structure of illite crystallinity is not irreversible with respect to temperature (Kubler, 1964), the temperature it indicates may not represent the thermal peak

but rather retrograde path. Similarly, the temperature derived from isotopic analyses (Kirschner et al., 1995) may not provide the maximal temperature, depending on the precise timing of vein formation versus peak temperature, and potential oxygen isotope later reequilibration. Thus, we believe that our data may provide a better image of the thermal structure at the temperature peak.

The thermal peak reached by the lowermost core of the Morcles nappe, with a maximum temperature of 358 °C, is consistent with the slightly higher thermal peak of 400 ± 25 °C determined in Alpine basement shear zones of the Mont Blanc Massif (Rolland et al., 2003).

In the Doldenhorn nappe, the T_{MAX} derived from our RSCM data (between 344 and 358 °C; Figures 5 and 8) are consistent with temperatures derived from calcite-graphite carbon isotope thermometry (between 318 and 385 °C, Herwegh & Pfiffner, 2005). As mentioned above, the latter may not all indicate the maximal temperature. Indeed, this geothermometer relies on ^{13}C fractionation between calcite and graphite and allows for temperature estimates between 300 and 800 °C with an error of ±15 °C (Herwegh & Pfiffner, 2005). The obtained temperatures do not necessarily correspond to the maximum temperature attained by the rocks, since fluid temperature can be in thermal disequilibrium with the host-rock temperature. However, Herwegh and Pfiffner (2005) do interpret these data as representing the T_{MAX} which is probably correct in this case and confirmed by our results.

Therefore, in order to have a more complete representation of the thermal structure of the Helvetic nappes (see next section), in the eastern Lower nappes (Doldenhorn nappe), RSCM T_{MAX} data were combined with these temperatures based on isotopic analysis. In areas where both the latter data and RSCM data have been obtained, a difference of approximately 25 °C can be observed (e.g., 318 °C vs. 353 °C, Figures 5 and 8), hence 10 °C larger than the internal, relative error inferred for our RSCM data. Because the two data sets are spatially separated (Figures 5 and 8), any discrepancy in the order of 25 °C would only affect the boundary region between these two data sets. Therefore, we consider that it is reasonable to combine them, being cautious when interpreting the boundary zone. The maps are interpreted in the next sections.

The thermal peak reached by the inner part of the Doldenhorn nappe, with a maximum T of 358 °C, is consistent with the slightly higher thermal peak of 450 ± 30 °C inferred for the basement (thermobarometric data, Fourcade et al., 1989; see also Challandes et al., 2008).

5.2. Thermal Structure and Its Relation to Tectonic Structures

Contouring all data in map view (Figure 5) shows a regular trend of iso-T_{MAX} lines. Except at the western margin of the Aar Massif, iso-T_{MAX} lines strike ENE from the Mt Blanc to the Aar Massif, crosscutting all major tectonic boundaries, and the absolute temperature systematically decreases from SE to NW.

The projection of the samples on the western and eastern cross sections and the contouring of their temperature show that the iso-T_{MAX} lines are folded but much less folded than the nappes themselves. In the western section (Figure 7c) an asymmetric antiformal structure with a subhorizontal limb in the SE and a subvertical limb in the NW is clearly visible (Figure 7c). An asymmetric antiformal structure is also observable in the eastern section (Figure 8c), although the subvertical limb is less developed. Both sections show, as already observed in map view, that the nappe boundaries are crosscut by the iso-T_{MAX} lines, indicating that the temperature peak was attained well after stacking of the nappes. Given that the upper nappes are entirely detached from their basements, it can be assumed that large amounts of displacements must have taken place before the peak of metamorphism was attained.

As best observable within the Morcles nappe (Figure 7), the iso-T_{MAX} lines are folded, but the amplitude of folding is by far smaller than the amplitude of the Morcles fold itself, which forms a recumbent isoclinal fold. Therefore, it can be argued that this lower nappe, which is still attached to its basement, was severely deformed before (or during, see below) the peak of metamorphism was reached. Even if the temperature data of Figure 7 are insufficient to constrain possible parasitic folds of the iso-T_{MAX} lines, as observed in all stratigraphic units of the Morcles nappe, line-length balancing of the folded iso-T_{MAX} lines indicates approximately 2–3 km of shortening (Figure 7c). This indicates that deformation continued well after the thermal peak. Indeed, NW directed thrusting is perfectly consistent with the folding of the iso-T_{MAX} lines from a subhorizontal, possibly gently north dipping orientation into the present asymmetric antiform with

a northwestern subvertical limb immediately above the major detachment plane (see next section for the shortening sequence, Figure 10).

The total shortening determined for the Morcles nappe is around 10 km (amount of shortening inferred for the external Mont Blanc Massif, forming the basement of the Morcles nappe, Boutoux et al., 2014). If, as suggested above, 2–3 km of shortening took place after the peak of metamorphism, possibly around 7 km occurred before the end of the thermal peak. Therefore, it can be concluded that the Morcles nappe, the youngest and lowest in the Helvetic stack, had already largely formed when postmetamorphic cooling initiated. These interpretations are consistent with Burkhard and Goy-Eggenberger (2001) and Kirschner et al. (1995) who inferred that the syndeformation veins and the formation of the nappes occurred at the temperature peak. This was also suggested in Herwegh and Pfiffner (2005).

The thermal peak recorded in the basement of the Mont Blanc Massif occurred between 30 and 17 Ma (Boutoux et al., 2016, and references therein) as for the Morcles nappes, where it is inferred to have occurred between 30 and 16 Ma (Kirschner et al., 1996). Cooling of the Aar Massif initiated between 20 and 22 Ma (Challandes et al., 2008), but the age of onset of the thermal peak there is still unknown. The age of the youngest sediments found in the Doldenhorn and Morcles nappes is about 30 Ma (Early Oligocene; Burkhard & Sommaruga, 1998; Pfiffner, 2014). Although it was suggested that the Rhone-Simplon Fault may offset the contact between Morcles nappe and Mont Blanc basement (Burkhard & Sommaruga, 1998), we follow most of the other interpretations (e.g., Escher et al., 1993; Pfiffner, 2011, 2012; Boutoux et al., 2016), indicating a continuity of the folded structures between basement and cover (Figure 10), suggesting coeval shortening of the Morcles nappe and the Mont Blanc basement. As basement deformation lies mainly between 30 and 17 Ma, coevally with the thermal peak, shortening attested by the Morcles nappe occurred mainly during the thermal peak. The complete shortening and thermal sequence is described in the next section (Figure 10).

The youngest sediments in the upper Helvetic nappes are slightly older (late Eocene-early Oligocene; Burkhard & Sommaruga, 1998) than in the lower Helvetic nappes. The stacking of the upper Helvetic nappes also occurred quickly, at around 30 Ma (Kirschner et al., 2003), before the onset of the thermal peak. The burial and heating of these nappes also occurred within a few million years. If the latter interpretations are correct, the emplacement of the Upper Helvetic nappes took place during increasing temperature conditions, but before the attainment of the metamorphic peak, whereas the lower Helvetic nappes (Morcles and Doldenhorn nappe) developed possibly before, mainly during but also after the peak of metamorphism. Considering that these structurally lower nappes were the last ones to form, their displacement probably initiated under higher-temperature conditions with respect to the upper Helvetic nappes. This conclusion may shed some light on the different tectonic style of the upper versus lower Helvetic nappes. Whereas the upper nappes are completely detached from their basement, the lower ones are sheared away from their basement to form a long, inverted fold limb, but they still remain attached to it in the core of this recumbent fold. This style difference reflects a smaller rheological contrast between basement and cover in the latter case, thus allowing for the deformation of both units at the same time and in the same place, in spite of different partitioning of deformation. Indeed, at temperatures above 300 °C, both the quartz-rich basement and the calcite-dominated cover are expected to deform in the ductile field (Brodie & Rutter, 2000; Mancktelow & Pennacchioni, 2010). Therefore, although the maximum values of temperature that affected the upper and lower nappes were similar (Figures 7 and 8), these temperatures were attained after deformation in the upper nappes, hence not affecting their deformation mechanisms and style. In contrast, a significant part of displacement of the lower nappes occurred under the peak temperature conditions assessed in Figures 7 and 8.

Finally, for the Niesen nappe only one T_{MAX} was obtained (261 °C, Figure 8). Although more data will be needed to confirm this, it indicates no jump in temperature between upper Helvetic nappes and the Valaisan domain. This result shows that the Penninic Thrust does not offset the thermal peak structure of the orogenic wedge, indicating that its activity predates the thermal peak.

5.3. Thermostructural Evolution

As reported above, it is noteworthy that our temperature data are consistent with the *P-T* peak inferred for the basement massifs. This observation is consistent with those made in the Lepontine Dome (Wiederkehr
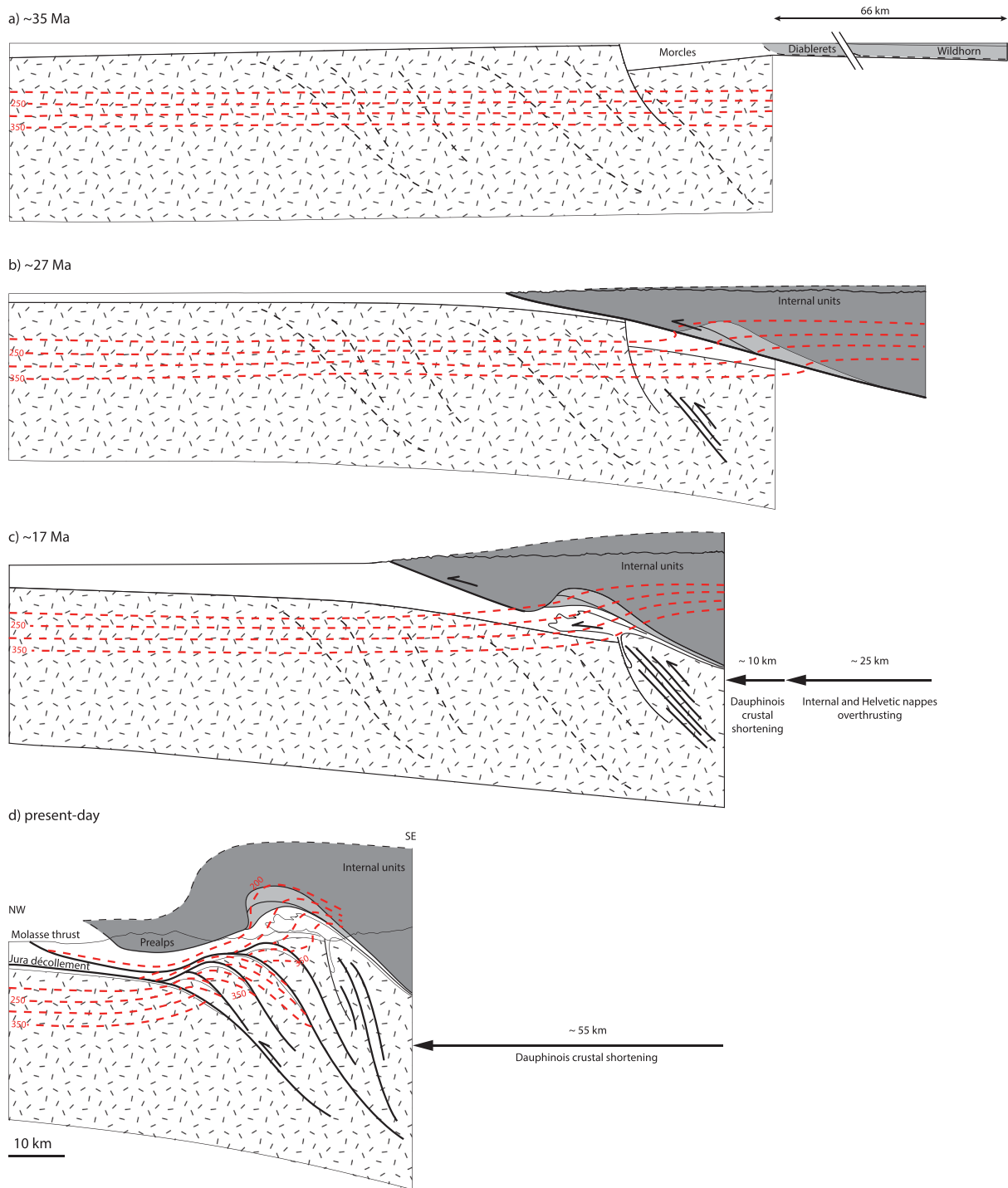
Figure 10. Shortening sequence of European proximal margin during the collisional Alpine phase zoomed in on the Helvetic nappe complex. As in Boutoux et al. (2016), we assume that the Rhône-Simplon transpressive dextral fault system does not significantly modify the collisional wedge thermal structure in this area. (a) Thirty-five million years, end of continental subduction and initiation of Alpine collision phase (see Price et al., 2018 for an alternative interpretation of the geodynamic setting). The youngest sediments of the future Helvetic nappes were deposited. (b) Twenty-seven million years, initiation of Helvetic nappe stacking with the upper Helvetic nappes stacked on the future Morcles nappe and initiation of the thermal peak. (c) Seventeen million years, initiation of the Dauphinois crustal shortening and both internal and Helvetic nappes overthrusting. End of the thermal peak and/or at the very beginning of the cooling history. (d) Present-day stage (modified after Burkhard & Sommaruga, 1998).

et al., 2011), showing that the iso-T_{MAX} lines of Barrovian metamorphism crosscut the Penninic Basal thrust, hence postdate the Penninic nappe stack. The age of the latter metamorphic event (18–19 Ma; Wiederkehr et al., 2009) coincides with the inferred initiation of cooling of the basement units underlying the Morcles nappes (Boutoux et al., 2016).

Moreover, the quasi-perfect lateral continuity between temperature of neighbor samples both in map and section view suggests that these temperatures affected the nappe stack synchronously. Thus, we can most likely assume that the geometry given by the iso-T_{MAX} lines provides a good image of the thermal structure for the Oligocene-Miocene time and that the iso-T_{MAX} lines represent isotherms. The geometric evolution of the isotherms in relation to the structural evolution of the Helvetic nappe stack can be linked to geochronological and thermochronological data visualized in the structural scenario (Figure 10).

From 35 to 30 Ma, the turbiditic sediments of the future Helvetic nappes were deposited (e.g., Burkhard & Sommaruga, 1998; Figure 10a). The thermal structure is relaxed, and the isotherms are flat (Figure 10a).

At about 27 Ma, the upper Helvetic nappes were stacked on the future Morcles nappe; that is, the latter was underthrusted below the wedge of the Internal Units (Figure 10b). Assuming that folding of the isotherms took place in response to folding at the orogen scale (e.g., Batt & Braun, 1997), but not at the nappe scale, we allow for a gentle climb of the isotherms toward the orogen interior (SE) (Figure 10b). Hence, subhorizontal iso-T_{MAX} lines are weakly deflected upward below and within the wedge of the internal zone, where the isotherms are inferred to crosscut the upper Helvetic nappe stack, starting from 27 Ma, that is, at a time when these nappes are already detached from their basement and thrust above the future Morcles nappe (Figure 10b). This geometry of the isotherms in this phase of collision stems from the observation that the iso-T_{MAX} lines crosscut all nappe boundaries.

Thermobarometric analyses of synkinematic phases in Alpine shear zones provide a P peak in the Mont-Blanc Massif at 5 ± 0.5 kbar and a T peak at 400 ± 25 °C (Rolland et al., 2003; Rossi et al., 2005), consistent with our data. Furthermore, shear zones in the Mont-Blanc and Aiguilles Rouges Massif were active from 30 to 14 Ma, as indicated by geochronologic data (Egli et al., 2016, 2017; Rolland et al., 2008; Cenki-Tok et al., 2013). Zircon fission track ages in the Mont Blanc Massif are in a range between 11.2 and 16 Ma (Fugenschuh & Schmid, 2003; Glotzbach et al., 2011; Seward & Mancktelow, 1994) and 17.2 Ma in the Aiguilles Rouges Massif, where partial resetting is inferred (Soom, 1990). The time gap between the age of ductile deformation and cooling ages suggests that cooling started around 17 Ma, following a nearly 10-Ma-long thermal peak (Boutoux et al., 2016). Figure 10c reflects the situation at the end of the thermal peak and/or at the very beginning of the cooling history. Between 27 and 17 Ma, we show an increase in the deflection of the isotherms, in line with increased underplating and erosion between 27 and 17 Ma. At 17 Ma, the iso-T_{MAX} lines crosscut the Morcles nappe limbs. As discussed above, the latter nappe formed during the thermal peak between 27 and 17 Ma.

In the Mont Blanc Massif, (U-Th-Sm)/He on zircon (ZHe) ages are younger than 9 Ma (Boutoux et al., 2016), apatite fission track ages are younger than 6.8 Ma (Fugenschuh & Schmid, 2003; Glotzbach et al., 2008; Leloup et al., 2005; Seward & Mancktelow, 1994; Soom, 1990), and apatite (AHe) ages are in the range 1.4–6.4 Ma (Glotzbach et al., 2008). These data are consistent and largely overlapping with those of the Aiguilles Rouges Massif, where apatite fission track ages are between 3.1 and 8.9 Ma (Leloup et al., 2005; Rahn, 1994; Seward & Mancktelow, 1994), ZHe ages between 3.9 and 7.8 Ma (Boutoux et al., 2016) and AHe ages between 4.4 and 6.7 Ma (Valla et al., 2012). These data indicate the continuous cooling, hence exhumation of the External Zone throughout the Neogene that is expressed by amplification of the antiforms in Figure 10d.

The closure temperature of zircon fission track is lower than the T_{MAX} determined for our samples that lie above the Mont Blanc and Aiguilles Rouges Massifs (>275 °C; Figure 7). Therefore, since 17 Ma, the RSCM-derived temperature data can be treated as passive markers that are displaced throughout the nappe stack, without modifying their fossil temperature values, hence illustrating folding of a paleo-isothermal structure. Indeed, Figure 10d shows a large bend where the iso-T_{MAX} lines crosscut the folded Morcles nappe that slightly continued deforming, thereby folding the iso-T_{MAX} lines, after 17 Ma. This is consistent with the fact that the Mont Blanc shear zone was active and accommodated some shortening after 17 Ma (e.g., Boutoux et al., 2016; Leloup et al., 2005; Rolland et al., 2008). The amplitude of folding manifested by the iso-T_{MAX}

lines is much smaller than that of the stratigraphic contacts, because the former was only affected by the last part of the deformation, namely, the one that took place since the beginning of cooling.

6. Conclusions

An extensive new set of T_{MAX} data obtained from RSCM on the sedimentary cover of the Alpine ECM in the Mont Blanc and the Aar Massifs shows that the thermal peak reached by the Helvetic nappes (lower and upper complexes) attained below 220 to 358 °C between the Mont Blanc and the Aar Massifs and 226 to 358 °C SW of the Mont Blanc Massif.

Thermal peak iso-T_{MAX} lines (i.e., most likely paleo-isotherms) are oblique with the folded layers and temperature decreases from SE to NW. Thus, the thermal peak and its associated thermal structure in the ECM sedimentary cover was acquired after most of the shortening of the Helvetic nappes and maintained for over 10 Ma (Boutoux et al., 2016). Therefore, the iso-T_{MAX} lines are only deformed by the last 2–3 km of shortening. Such paleo-isotherm deformation attest for postthermal peak shortening.

Finally, we show that the upper Helvetic nappes were emplaced before their thermal peak, thus at relatively low temperature (probably less than 300 °C), which explains the fact that they are detached from their basement. On the contrary, the lower nappes (e.g., Morcles nappe) initiated deformation before attaining the peak of metamorphism, but mainly during this long lasting peak (Boutoux et al., 2016), and partly even after its termination. The relatively high temperatures (300–350 °C) attained along the base of the Morcles nappe, explain the fact the basement cover did not act as a strong rheological contrast.

References

Batt, G. E., & Braun, J. (1997). On the thermomechanical evolution of compressional orogens. *Geophysical Journal International*, *128*(2), 364–382. https://doi.org/10.1111/j.1365-246X.1997.tb01561.x

Bauville, A., & Schmalholz, S. M. (2015). Transition from thin-to thick-skinned tectonics and consequences for nappe formation: Numerical simulations and applications to the Helvetic nappe system, Switzerland. *Tectonophysics*, *665*, 101–117. https://doi.org/10.1016/j.tecto.2015.09.030

Beaumont, C., Fullsack, P., & Hamilton, J. (1994). Styles of crustal deformation in compressional orogens caused by subduction of the underlying lithosphere. *Tectonophysics*, *232*(1-4), 119–132. https://doi.org/10.1016/0040-1951(94)90079-5

Bellahsen, N., Jolivet, L., Lacombe, O., Bellanger, M., Boutoux, A., Garcia, S., et al. (2012). Mechanisms of margin inversion in the external Western Alps: Implications for crustal rheology. *Tectonophysics*, *560*, 62–83. https://doi.org/10.1016/j.tecto.2012.06.022

Bellahsen, N., Mouthereau, F., Boutoux, A., Bellanger, M., Lacombe, O., Jolivet, L., & Rolland, Y. (2014). Collision kinematics in the western external Alps: Kinematics of the Alpine collision. *Tectonics*, *33*, 1055–1088. https://doi.org/10.1002/2013TC003453

Bellanger, M., Augier, R., Bellahsen, N., Jolivet, L., Monié, P., Baudin, T., & Beyssac, O. (2015). Shortening of the European Dauphinois margin (Oisans Massif, Western Alps): New insights from RSCM maximum temperature estimates and ^{40}Ar/^{39}Ar in situ dating. *Journal of Geodynamics*, *83*, 37–64. https://doi.org/10.1016/j.jog.2014.09.004

Beyssac, O., Bollinger, L., Avouac, J.-P., & Goffé, B. (2004). Thermal metamorphism in the lesser Himalaya of Nepal determined from Raman spectroscopy of carbonaceous material. *Earth and Planetary Science Letters*, *225*(1–2), 233–241. https://doi.org/10.1016/j.epsl.2004.05.023

Beyssac, O., Goffé, B., Chopin, C., & Rouzaud, J. N. (2002). Raman spectra of carbonaceous material in metasediments: A new geothermometer. *Journal of Metamorphic Geology*, *20*(9), 859–871. https://doi.org/10.1046/j.1525-1314.2002.00408.x

Beyssac, O., Goffé, B., Petitet, J.-P., Froigneux, E., Moreau, M., & Rouzaud, J.-N. (2003). On the characterization of disordered and heterogeneous carbonaceous materials by Raman spectroscopy. *Spectrochimica Acta Part A: Molecular and Biomolecular Spectroscopy*, *59*(10), 2267–2276. https://doi.org/10.1016/S1386-1425(03)00070-2

Beyssac, O., Rouzaud, J.-N., Goffé, B., Brunet, F., & Chopin, C. (2002). Graphitization in a high-pressure, low-temperature metamorphic gradient: A Raman microspectroscopy and HRTEM study. *Contributions to Mineralogy and Petrology*, *143*(1), 19–31. https://doi.org/10.1007/s00410-001-0324-7

Bousquet, R., Oberhänsli, R., Goffé, B., Wiederkehr, M., Koller, F., Schmid, S. M., et al. (2008). Metamorphism of metasediments at the scale of an orogen: A key to the Tertiary geodynamic evolution of the Alps. *Geological Society, London, Special Publications*, *298*(1), 393–411. https://doi.org/10.1144/SP298.18

Boutoux, A., Bellahsen, N., Lacombe, O., Verlaguet, A., & Mouthereau, F. (2014). Inversion of pre-orogenic extensional basins in the external Western Alps: Structure, microstructures and restoration. *Journal of Structural Geology*, *60*, 13–29. https://doi.org/10.1016/j.jsg.201312.014

Boutoux, A., Bellahsen, N., Nanni, U., Pik, R., Verlaguet, A., Rolland, Y., & Lacombe, O. (2016). Thermal and structural evolution of the external Western Alps: Insights from (U–Th–Sm)/He thermochronology and RSCM thermometry in the Aiguilles Rouges/Mont Blanc massifs. *Tectonophysics*, *683*, 109–123. https://doi.org/10.1016/j.tecto.2016.06.010

Brodie, K. H., & Rutter, E. H. (2000). Deformation mechanisms and rheology: Why marble is weaker than quartzite. *Journal of the Geological Society, London*, *157*, 1093–1096.

Broquet P., Gidon M., Monjuvent G. (1987). Carte géologique de la France au 1/250000. Feuille n°25: Thonon-Les-Bains et notice explicative. Publi. BRGM.

Bucher, S., Ulardic, C., Bousquet, R., Ceriani, S., Fügenschuh, B., Gouffon, Y., & Schmid, S. M. (2004). Tectonic evolution of the Briançonnais units along a transect (ECORS-CROP) through the Italian-French Western Alps. *Eclogae Geologicae Helvetiae*, *97*(3), 321–345. https://doi.org/10.1007/s00015-004-1139-0

Burkhard, M., (1988). L'Helvétique de la bordure occidentale du massif de l'Aar (évolution tectonique et métamorphique). Eclogae Geol. Helv. 81/1, 63-114

Burkhard, M., & Goy-Eggenberger, D. (2001). Near vertical iso-illite-crystallinity surfaces cross-cut the recumbent fold structure of the Morcles nappe, Swiss Alps. *Clay Minerals*, *36*(2), 159–170. https://doi.org/10.1180/000985501750177906

Burkhard, M., & Sommaruga, A. (1998). Evolution of the western Swiss Molasse basin: structural relations with the Alps and the Jura belt. *Geological Society, London, Special Publications*, *134*(1), 279–298. https://doi.org/10.1144/GSL.SP.1998.134.01.13

Cenki-Tok, B., Darling, J. R., Rolland, Y., Dhuime, B., & Storey, C. D. (2013). Direct dating of mid-crustal shear zones with synkinematic allanite: New in situ U–Th–Pb geochronological approaches applied to the Mont Blanc massif. *Terra Nova*, *26*, 29–37. https://doi.org/10.1111/ter.12066

Ceriani, S., & Schmid, S. M. (2004). From NS collision to WNW-directed post-collisional thrusting and folding: Structural study of the Frontal Penninic Units in Savoie (Western Alps, France). *Eclogae Geologicae Helvetiae*, *97*(3), 347–369.

Challandes, N., Marquer, D., & Villa, I. M. (2008). P-T-t modelling, fluid circulation, and ^{39}Ar-^{40}Ar and Rb-Sr mica ages in the Aar Massif shear zones (Swiss Alps). *Swiss Journal of Geosciences*, *101*(2), 269–288. https://doi.org/10.1007/s00015-008-1260-6

Chopin, C. (1987). Very-high-pressure metamorphism in the Western Alps: Implications for subduction of continental crust [and Discussion]. Philosophical Transactions of the Royal Society of London. *Series A, Mathematical and Physical Sciences*, *321*(1557), 183–197. https://doi.org/10.1098/rsta.1987.0010

Crouzet, C., Ménard, G., & Rochette, P. (1999). High-precision three-dimensional paleothermometry derived from paleomagnetic data in an Alpine metamorphic unit. *Geology*, *27*(6), 503–506. https://doi.org/10.1130/0091-7613(1999)027<0503:HPTDPD>2.3.CO;2

Debelmas J., Bellière J., von Raumer J., Rosset J., Charollais J., Barféty J.C., et al., 1980. Carte géologique de la France au 1/250000. Feuille n° 30: Annecy et notice explicative. Publi. BRGM

Dumont, T., Champagnac, J.-D., Crouzet, C., & Rochat, P. (2008). Multistage shortening in the Dauphiné zone (French Alps): The record of Alpine collision and implications for pre-Alpine restoration. *Swiss Journal of Geosciences*, *101*(1), 89–110. https://doi.org/10.1007/s00015-008-1280-2

Dumont, T., Schwartz, S., Guillot, S., Simon-Labric, T., Tricart, P., & Jourdan, S. (2012). Structural and sedimentary records of the Oligocene revolution in the Western Alpine arc. *Journal of Geodynamics*, *56*, 18–38. https://doi.org/10.1016/j.jog.2011.11.006

Egli, D., & Mancktelow, N. (2013). The structural history of the Mont Blanc massif with regard to models for its recent exhumation. *Swiss journal of geosciences*, *106*(3), 469–489.

Egli, D., Mancktelow, N., & Spikings, R. (2017). Constraints from 40Ar/39Ar geochronology on the timing of Alpine shear zones in the Mont Blanc-Aiguilles Rouges region of the European Alps. *Tectonics*, *36*, 730–748. https://doi.org/10.1002/2016TC004450

Egli, D., Müller, W., & Mancktelow, N. (2016). Laser-cut Rb–Sr microsampling dating of deformational events in the Mont Blanc-Aiguilles Rouges region (European Alps). *Terra nova*, *28*(1), 35–42.

Engi, M., Berger, A., & Roselle, G. T. (2001). Role of the tectonic accretion channel in collisional orogeny. *Geology*, *29*(12), 1143–1146. https://doi.org/10.1130/0091-7613(2001)029<1143:ROTTAC>2.0.CO;2

Escher, A., Masson, H., & Steck, A. (1993). Nappe geometry in the western Swiss Alps. *Journal of Structural Geology*, *15*(3–5), 501–509. https://doi.org/10.1016/0191-8141(93)90144-Y

Fourcade, S., Marquer, D., & Javoy, M. (1989). 18O16O variations and fluid circulation in a deep shear zone: The case of the Alpine ultramylonites from the Aar massif (central Alps, Switzerland). *Chemical geology*, *77*(2), 119–131. https://doi.org/10.1016/0009-2541(89)90137-X

Fugenschuh, B., & Schmid, S. M. (2003). Late stages of deformation and exhumation of an orogen constrained by fission-track data: A case study in the Western Alps. *Geological Society of America Bulletin*, *115*(11), 1425–1440. https://doi.org/10.1007/s00015-004-1113-x

Glotzbach, C., Reinecker, J., Danišík, M., Rahn, M., Frisch, W., & Spiegel, C. (2008). Neogene exhumation history of the Mont Blanc massif, western Alps. *Tectonics*, *27*, TC4011. https://doi.org/10.1029/2008TC002257

Glotzbach, C., Reinecker, J., Danišík, M., Rahn, M. K., Frisch, W., & Spiegel, C. (2010). Thermal history of the central Gotthard and Aar massifs, European Alps: Evidence for steady state, long-term exhumation. *Journal of Geophysical Research*, *115*, F03017. https://doi.org/10.1029/2009JF001304

Glotzbach, C., van der Beek, P. A., & Spiegel, C. (2011). Episodic exhumation and relief growth in the Mont Blanc massif, Western Alps from numerical modelling of thermochronology data. *Earth and Planetary Science Letters*, *304*, 417–430. https://doi.org/10.1016/j.epsl.2011.02.020

Goncalves, P., Oliot, E., Marquer, D., & Connolly, J. A. D. (2012). Role of chemical processes on shear zone formation: an example from the Grimsel metagranodiorite (Aar massif, central Alps). *Journal of Metamorphic Geology*, *30*(7), 703–722. https://doi.org/10.1111/j.1525-1314.2012.00991.x

Groshong, R. H. Jr., Pfiffner, O. A., & Pringle, L. R. (1984). Strain partitioning in the Helvetic thrust belt of eastern Switzerland from the leading edge to the internal zone. *Journal of Structural Geology*, *6*(1-2), 5–18. https://doi.org/10.1016/0191-8141(84)90079-8

Herwegh, M., & Pfiffner, O. A. (2005). Tectono-metamorphic evolution of a nappe stack: A case study of the Swiss Alps. *Tectonophysics*, *404*(1–2), 55–76. https://doi.org/10.1016/j.tecto.2005.05.002

Huerta, A. D., Royden, L. H., & Hodges, K. V. (1996). The interdependence of deformational and thermal processes in mountain belts. *Science*, *273*(5275), 637–639. https://doi.org/10.1126/science.273.5275.637

Huerta, A. D., Royden, L. H., & Hodges, K. V. (1998). The thermal structure of collisional orogens as a response to accretion, erosion, and radiogenic heating. *Journal of Geophysical Research*, *103*(B7), 15,287–15,302. https://doi.org/10.1029/98JB00593

Huggenberger, P. (1985). Faltenmodelle und Verformungsverteilung in Deckenstrukturen am Beispiel der Morcles-Decke (Helvetikum der Westschweiz) (Doctoral dissertation, ETH Zurich). https://doi.org/10.3929/ethz-a-000365939

Jamieson, R. A., Beaumont, C., Fullsack, P., Treloar, P. J., & O'Brien, P. (1998). What controls regional metamorphism in orogens? Insights from thermal and mechanical models. *Electronic Geosciences*.

Jamieson, R. A., Beaumont, C., Hamilton, J., & Fullsack, P. (1996). Tectonic assembly of inverted metamorphic sequences. *Geology*, *24*(9), 839–842.

Kempf, O., & Pfiffner, O. A. (2004). Early Tertiary evolution of the North Alpine Foreland Basin of the Swiss Alps and adjoining areas. *Basin Research*, *16*(4), 549–567.

Kirschner, D. L., Cosca, M. A., Masson, H., & Hunziker, J. C. (1996). Staircase 40/Ar39Ar spectra of fine-grained white mica: Timing and duration of deformation and empirical constraints on argon diffusion. *Geology*, *24*(8), 747–750. https://doi.org/10.1130/0091-7613(1996)024<0747:SAASOF>2.3.CO;2

Kirschner, D. L., Masson, H., & Cosca, M. A. (2003). An $^{40}Ar/^{39}Ar$, Rb/Sr, and stable isotope study of micas inlow-grade fold-and-thrust belt: An example from the Swiss Helvetic Alps. *Contributions to Mineralogy and Petrology*, *145*(4), 460–480. https://doi.org/10.1007/s00410-003-0461-2

Kirschner, D. L., Sharp, Z. D., & Masson, H. (1995). Oxygen isotope thermometry of quartz-calcite veins: Unraveling the thermal-tectonic history of the subgreenschist facies Morcles nappe (Swiss Alps). *Geological Society of America Bulletin*, *107*(10), 1145–1156. https://doi.org/10.1130/0016-7606(1995)107

Konstantinovskaia, E., & Malavieille, J. (2005). Erosion and exhumation in accretionary orogens: Experimental and geological approaches. *Geochemistry, Geophysics, Geosystems*, *6*, Q02006. https://doi.org/10.1029/2004GC000794

Kubler, B. (1964). Les argiles, indicateurs de métamorphisme. *Revue de l'Institut Francais du Petrole*, *19*, 1093–1112.

Lafosse, M., Boutoux, A., Bellahsen, N., & Le Pourhiet, L. (2016). Role of tectonic burial and temperature on the inversion of inherited extensional basins during collision. *Geological Magazine*, *153*(5-6), 811–826. https://doi.org/10.1017/S0016756816000510

Lahfid, A., Beyssac, O., Deville, E., Negro, F., Chopin, C., & Goffé, B. (2010). Evolution of the Raman spectrum of carbonaceous material in low-grade metasediments of the Glarus Alps (Switzerland): RSCM in low-grade metasediments. *Terra Nova*, *22*(5), 354–360. https://doi.org/10.1111/j.1365-3121.2010.00956.x

Leloup, P. H., Arnaud, N., Sobel, E. R., & Lacassin, R. (2005). Alpine thermal and structural evolution of the highest external crystalline massif: Exhumation of the Mont-Blanc massif. *Tectonics*, *24*, TC4002. https://doi.org/10.1029/2004TC001676

Lemoine, M., Bas, T., Arnaud-Vanneau, A., Arnaud, H., Dumont, T., Gidon, M., et al. (1986). The continental margin of the Mesozoic Tethys in the western Alps. *Marine and petroleum geology*, *3*(3), 179–199. https://doi.org/10.1016/0264-8172(86)90044-9

Liao, J., Gerya, T., & Malusà, M. G. (2018). 3D modeling of crustal shortening influenced by along-strike lithological changes: Implications for continental collision in the Western and central Alps. *Tectonophysics*, *746*, 425–438. https://doi.org/10.1016/j.tecto.2018.01.031

Mancktelow, N. S., & Pennacchioni, G. (2010). Why calcite can be stronger than quartz? *Journal of Geophysical Research*, *115*, B01402. https://doi.org/10.1029/2009JB006526

Michalski, I., & Soom, M. (1990). The Alpine thermo-tectonic evolution of the Aar and Gotthard massifs, central Switzerland: Fission track ages on zircon and apatite and K-Ar mica ages. *Schweizerische Mineralogische und Petrographische Mitteilungen*, *70*, 373–387.

Nibourel, L., Berger, A., Egli, D., Luensdorf, N. K., & Herwegh, M. (2018). Large vertical displacements of a crystalline massif recorded by Raman thermometry. *Geology*, *46*(10), 879–882.

Pfiffner, O. A. (1993). The structure of the Helvetic nappes and its relation to the mechanical stratigraphy. *Journal of Structural Geology*, *15*(3–5), 511–521. https://doi.org/10.1016/0191-8141(93)90145-Z

Pfiffner, O. A. (2011) Structural map of the Helvetic zone of the Swiss Alps including Vorarlberg (Austria) and Haute Savoie (France), Explanatory notes, Geological Special Map 1:100'000, No. 128/1, Swiss Geological Survey.

Pfiffner, O. A. (2014). *Geology of the Alps*. New York, USA: John Wiley & Sons.

Pfiffner, O. A., Burkhard, M., Haenni, R., Kammer, A., Kligfield, R., Mancktelow, N. S., et al. (2010). Structural map of the Helvetic zone of the Swiss Alps, including Vorarlberg (Austria) and Haute Savoie (France), Sheet 45 Haute Savoie. Geological Special Map 1:100'000, No. 128/1, Swiss Geological Survey.

Piccolo, A., Faccenda, M., Carosi, R., Montomoli, C., & Visonà, D. (2017). Crustal strength control on structures and metamorphism in collisional orogens. *Tectonophysics*, *746*, 470–492. https://doi.org/10.1016/j.tecto.2017.09.018

Price, J. B., Wernicke, B. P., Cosca, M. A., & Farley, K. A. (2018). Thermochronometry Across the Austroalpine-Pennine Boundary, central Alps, Switzerland: Orogen-perpendicular normal fault slip on a major "overthrust" and its implications for orogenesis. *Tectonics*, *37*, 724–757. https://doi.org/10.1002/2017TC004619

Rahn, M. (2001). The metamorphic and exhumation history of the Helvetic Alps, Switzerland, as revealed by apatite and zircon fission tracks (Habilitation thesis).

Rahn, M.K. (1994). Incipient metamorphism of the Glarus Alps: Petrology of the Taveyanne Greywacke and fission track dating (Ph-D Thesis) Univ. of Basel, Basel, Switzerland.

Ramsay, J. G., & Huber, M. I. (1987). *The techniques of modern structural geology*, (Vol. 2, p. 392). London, UK: Academic press.

Rolland, Y., Rossi, M., Cox, S. F., Corsini, M., Mancktelow, N., Pennacchioni, G., et al. (2008). 40Ar/39Ar dating of synkinematic white mica: Insights from fluid-rock reaction in low-grade shear zones (Mont Blanc Massif) and constraints on timing of deformation in the NW external Alps. *Geological Society, London, Special Publications*, *299*(1), 293–315. https://doi.org/10.1144/SP299.18

Rolland, Y., Cox, S., Boullier, A.-M., Pennacchioni, G., & Mancktelow, N. (2003). Rare earth and trace element mobility in mid-crustal shear zones: Insights from the Mont Blanc Massif (western Alps). *Earth and Planetary Science Letters*, *214*(1–2), 203–219. https://doi.org/10.1016/S0012-821X(03)00372-8

Rolland, Y., Cox, S. F., & Corsini, M. (2009). Constraining deformation stages in brittle–ductile shear zones from combined field mapping and $^{40}Ar/^{39}Ar$ dating: The structural evolution of the Grimsel Pass area (Aar Massif, Swiss Alps). *Journal of Structural Geology*, *31*(11), 1377–1394. https://doi.org/10.1016/j.jsg.2009.08.003

Rosenberg, C. L., & Berger, A. (2009). On the causes and modes of exhumation and lateral growth of the Alps. *Tectonics*, *28*, TC6001. https://doi.org/10.1029/2008TC002442

Rossi, M., Rolland, Y., Vidal, O., & Cox, S. F. (2005). Geochemical variations and element transfer during shear zone development and related episyenites at middle crust depths: insights from the study of the Mont-Blanc Granite (French–Italian Alps). *Geological Society London Special Publications*, *245*, 373–396.

Schmid, S. M., Pfiffner, O. A., Froitzheim, N., Schönborn, G., & Kissling, E. (1996). Geophysical-geological transect and tectonic evolution of the Swiss-Italian Alps. *Tectonics*, *15*, 1036–1064. https://doi.org/10.1029/96TC00433

Seward, D., & Mancktelow, N. S. (1994). Neogene kinematics of the central and Western Alps: Evidence from fission-track dating. *Geology*, *22*(9), 803–806. https://doi.org/10.1130/0091-7613(1994)022b0803:NKOTCAN2.3.CO;2

Sinclair, H. D. (1997). Tectonostratigraphic model for underfilled peripheral foreland basins: An Alpine perspective. *Geological Society of America Bulletin*, *109*(3), 324–346. https://doi.org/10.1130/0016-7606(1997)109<0324:TMFUPF>2.3.CO;2

Soom, M.A., (1990). Abkiihlungs—und Hebungsgeschichte der Extemmas—sive und der penninischen Decken beidseits der Simplon-Rhone-Linie seit dem Oligoziin: Spaltspurdatierungen an Apatit/Zircon und K–Ar—Datierungen an Biotit/Muskowit (Westliche Zentralalpen) (Ph-D Thesis) University of Bern, Switzerland.

Stampfli, G. M., Borel, G. D., Marchant, R., & Mosar, J. (2002). Western Alps geological constraints on western Tethyan reconstructions. *Journal of the Virtual Explorer*, *8*, 77.

Steck, A., Della Torre, F., Keller, F., Pfeifer, H. R., Hunziker, J., & Masson, H. (2013). Tectonics of the Lepontine Alps: ductile thrusting and folding in the deepest tectonic levels of the Central Alps. *Swiss Journal of Geosciences*, *106*, 427–450. https://doi.org/10.1007/s00015-013-0135-7

Stockmal, G. S., Beaumont, C., Nguyen, M., & Lee, B. (2007). Mechanics of thin-skinned fold-and-thrust belts: Insights from numerical models. *Geological Society of America Special Papers*, *433*, 63–98.

Todd, C. S., & Engi, M. (1997). Metamorphic field gradients in the central Alps. *Journal of Metamorphic Geology*, *15*(4), 513–530. https://doi.org/10.1111/j.1525-1314.1997.00038.x

University of Bern and FWOG: Geological map of Switzerland 1:500000 (2005). Swisstopo, Bern, Switzerland, ISBN 3-906723-39-9.

University of Bern and FWOG: Tectonic Map of Switzerland 1:500 000 (2005). Swisstopo, Bern, Switzerland, ISBN 3-906723-56-9.

Valla, P. G., van der Beek, P. A., Shuster, D. L., Braun, J., Herman, F., Tassan-Got, L., & Gautheron, C. (2012). Late Neogene exhumation and relief development of the Aar and Aiguilles Rouges massifs (Swiss Alps) from low-temperature thermochronology modeling and 4He/3He thermochronometry. *Journal of Geophysical Research*, *117*, F01004. https://doi.org/10.1029/2011JF002043

Vanderhaeghe, O., Medvedev, S., Fullsack, P., Beaumont, C., & Jamieson, R. A. (2003). Evolution of orogenic wedges and continental plateaux: Insights from crustal thermal–mechanical models overlying subducting mantle lithosphere. *Geophysical Journal International*, *153*(1), 27–51. https://doi.org/10.1046/j.1365-246X.2003.01861.x

von Tscharner, M., Schmalholz, S. M., & Epard, J.-L. (2016). 3-D numerical models of viscous flow applied to fold nappes and the Rawil depression in the Helvetic nappe system (western Switzerland). *Journal of Structural Geology*, *86*, 32–46. https://doi.org/10.1016/j.jsg.2016.02.007

Wiederkehr, M., Bousquet, R., Ziemann, M. A., Berger, A., & Schmid, S. M. (2011). 3-D assessment of peak-metamorphic conditions by Raman spectroscopy of carbonaceous material: an example from the margin of the Lepontine dome (Swiss central Alps). *International journal of earth sciences*, *100*(5), 1029–1063. https://doi.org/10.1007/s00531-010-0622-2

Wiederkehr, M., Sudo, M., Bousquet, R., Berger, A., & Schmid, S. M. (2009). Alpine orogenic evolution from subduction to collisional thermal overprint: The ^{40}Ar/^{39}Ar age constraints from the Valaisan Ocean, central Alps. *Tectonics*, *28*, TC6009. https://doi.org/10.1029/2009TC002496

Yamato, P., Kaus, B. J. P., Mouthereau, F., & Castelltort, S. (2011). Dynamic constraints on the crustal-scale rheology of the Zagros fold belt, Iran. *Geology*, *39*(9), 815–818. https://doi.org/10.1130/G32136.1

Erratum

In the originally published version of this article, an incorrect copy of Figure 7 published. The figure has since been corrected, and this version may be considered the authoritative version of record.